

A jet-cloud interaction in the 3C 196 environment ^{★,★★}

L. Christensen^{1,2}, K. Jahnke^{1,3}, L. Wisotzki¹, S. F. Sánchez^{1,4}, K. Exter⁵, and M. M. Roth¹

¹ Astrophysikalisches Institut Potsdam, An der Sternwarte 16, 14482 Potsdam, Germany
e-mail: lchrist@eso.org

² European Southern Observatory, Casilla 19001, Santiago 19, Chile

³ Max Planck Institut für Astronomie, Königstuhl 17, 69117 Heidelberg, Germany

⁴ Centro Astronomico Hispano Aleman de Calar Alto, Spain

⁵ Instituto de Astrofísica de Canarias, La Laguna, Tenerife, Spain

Received 24 November 2005 / Accepted 7 March 2006

Abstract. Powerful radio galaxies and radio-loud quasars at high redshifts are frequently associated with extended emission-line regions (EELRs). Here we investigate the [O II] EELR around the quasar 3C 196 at $z = 0.871$ using integral field spectroscopy. We also detect extended [Ne II] emission at a distance of about 30 kpc from the core. The emission is aligned with the radio hot spots and shows a redshifted and a blueshifted component with a velocity difference of ~ 800 km s $^{-1}$. The alignment effect and large velocities support the hypothesis that the EELR is caused by a jet-cloud interaction, which is furthermore indicated by the presence of a pronounced bend in the radio emission at the location of the radio hot spots. We also report observations of two other systems which do not show as clear indications of interactions. We find a weaker alignment of an [O II] EELR from the $z = 0.927$ quasar 3C 336, while no EELR is found around the core-dominated quasar OI 363 at $z = 0.63$.

Key words. Galaxies: kinematics and dynamics – quasars: emission lines – quasars: individual: 3C 196

1. Introduction

Interactions of powerful radio emission with surrounding gas can explain the presence of extended optical emission line regions around high redshift, radio-loud AGN. However, most studies have focused on radio galaxies (e.g. Villar-Martin et al. 1997), rather than radio-loud quasars (RLQs), because there is no bright optical glare from the central AGN itself. In the case of broad absorption-line quasars, measurements of the blue shifted absorption lines have shown large outflow velocities (Turnshek 1984), but only a few observations have revealed a direct connection between the more extended gas and the central engine. Outflows driven by AGN activity are potentially an effective method for quenching star formation in the host galaxy (Di Matteo et al. 2005).

Luminous extended narrow emission-line regions (EELRs), reaching more than 100 kpc from the QSO nucleus, have been detected around quasars at redshifts between 1 and 4 (e.g. Heckman et al. 1991; Bremer et al. 1992a,b). At low redshift,

detailed analyses of the host galaxies are enhanced by observations of the stellar continuum emission, and in several cases the line emission extends much farther than the continuum emission. Aside from interaction with the radio emission, possible explanations include photoionisation from the central source, or ionising radiation from massive stars in star-forming regions in the host galaxy. The interaction scenario is supported by observations of alignment of the radio jets with the optical continuum and extended emission line regions in a sample of radio galaxies (McCarthy et al. 1987). Such interactions result in shocks which compress and heat the gas, and subsequent recombination line emission will cool the material. As alternative explanations for EELRs, remnants from galaxy mergers (Stockton & MacKenty 1987), material falling into dark matter potentials (Haiman & Rees 2001), or cooling flows in massive galaxy clusters (e.g. Fabian & Crawford 1990) have been suggested.

These scenarios make different predictions for the surrounding material, and so the morphologies and kinematics of the EELRs can be used to discriminate between them. To investigate the structure and kinematics of these EELRs, narrow- and broad-band images, and slit spectroscopy have traditionally been used. Integral field spectroscopy (IFS) presents an alternative technique that allows imaging and spectroscopy simultaneously. IFS of six RLQs at redshift $0.26 < z < 0.60$ showed that EELRs are common, although not always aligned with the radio axis (Crawford & Vanderriest 2000).

Send offprint requests to: L. Christensen

* Based on observations made with the WHT operated on the island of La Palma by the Isaac Newton Group in the Spanish Observatorio del Roque de los Muchachos of the Instituto de Astrofísica de Canarias

** Based on observations obtained at the German-Spanish Astronomical Center, Calar Alto, operated by the Max-Planck-Institut für Astronomie Heidelberg jointly with the Spanish National Commission for Astronomy.

An alignment between the radio axis and the extended emission around one lobe-dominated quasar was reported (Bremer 1997), and later IFS gave evidence for a jet-cloud interaction (Crawford & Vanderriest 1997). At $z > 2$, detections of extended [O II] and [O III] emission lines have indicated no strong evolution with redshift, and a tendency for stronger line emission to be spatially coincident with the stronger radio emission (Wilman et al. 2000).

The AGN unification scheme states that radio galaxies and RLQs are the same objects viewed at different angles relative to their jets (Barthel 1989). IFS of radio galaxies have also indicated jet-cloud interactions through the alignment effect and kinematics (Márquez et al. 2000; Solórzano-Iñarrea & Tadhunter 2003; Sánchez et al. 2004). Like the EELRs from RLQs, the alignment is roughly consistent with the radio morphology (McCarthy et al. 1987). This alignment effect for RLQs and the EELRs is also found at higher redshifts, but it is not as well-determined at $z > 2$ (Heckman et al. 1991; Hutchings 1992), possibly due to resonance scattering of Ly α photons.

This paper presents observations of three RLQs at $0.6 < z < 0.9$ and the first analysis of the alignment effect of the EELRs in this redshift range using IFS.

2. Observations and data reduction

The data were obtained in connection with a project aimed at detecting emission from galaxies associated with intervening damped Lyman- α absorption lines (Christensen et al. 2004, 2005). From the original sample of seven QSOs at $z < 2$, only three RLQs have redshifted strong optical emission lines within the wavelength range of the observations.

The observations were carried out with two integral field spectrographs; INTEGRAL (Arribas et al. 1998) mounted on the 4m William Herschel Telescope, La Palma, and the Potsdam Multi Aperture Spectrophotometer (PMAS) mounted on the 3.5m telescope at Calar Alto (Roth et al. 2000, 2005). Table 1 presents a log of the observations.

2.1. INTEGRAL observations

The observations were obtained with the SB2 fibre bundle, which consists of 189 object fibres plus 30 sky fibres arranged in a ring with a diameter of $90''$. Each fibre has a diameter of $0''.9$ on the sky, giving a main field of view of $12'' \times 16''$ with a non-contiguous sampling and a filling factor of about 67%. We used a $600 \text{ lines mm}^{-1}$ grating with a dispersion of 3 \AA pixel^{-1} and a spectral resolution of 6 \AA measured from the width of sky emission lines.

Data reduction was performed using IRAF tasks modified specifically for the reduction of INTEGRAL data (see Garcia-Lorenzo et al. 2005). Bias frames were subtracted and the frames were cleaned for cosmic ray hits using the algorithm described in Pych (2004). All spectra were extracted using the trace of the 219 spectra on the CCD found from an exposure of a continuum lamp obtained at the beginning of the night. Wavelength calibration was done using spectra of emission line lamps also extracted for each fibre. The RMS deviation of the

wavelength for sky emission lines for each spectrum was determined to be $<0.2 \text{ \AA}$. Differences between the individual fibre transmissions as a function of wavelength were corrected for by modeling the transmission of sky flat frames obtained at twilight. Two regions on the CCD were affected by scattered light but there only in the blue end of the spectral range and only affecting some of the spectra. Otherwise, scattered light was found to be negligible compared to the overall read noise of the CCD. Some sky fibres are contaminated by the QSO flux because they are located next to the QSO spectra on the CCD, and therefore affected by cross talk. The sky fibres were examined, and those uncontaminated by the QSO flux were averaged and subtracted from each object spectrum. We do not expect that any extended line emission region is present at a distance of $45''$. To facilitate inspection and visualisation, the data were interpolated onto a cube of square spaxels (spatial elements) with sizes of $0''.3 \times 0''.3$. This interpolation and further visualization of the data cubes was done with the Euro3D visualization tool (Sánchez 2004). When one-dimensional spectra are extracted, we retain the original spaxels sizes, instead using the interpolated data cube.

2.2. PMAS observations

PMAS has 16×16 fibres coupled to a lens array and has a contiguous sampling of the sky. The effective size of each lens is square with a size of $0''.5$ on a side. The instrument configuration used provided a field of view of $8'' \times 8''$ and using a grating with $300 \text{ lines mm}^{-1}$ resulted in a spectral resolution of 6.6 \AA .

The method for reducing PMAS data was essentially the same as for INTEGRAL data and was done with our own IDL-based software package P3d (Becker 2002). The main difference was the sky subtraction because PMAS does not have allocated sky fibres. Instead, an average sky spectrum was created from spectra at the edge of the field of view uncontaminated by the QSO or the nebulae. Because the spatial position of the nebulae was previously unknown, several different selections of sky spectra were examined before selecting an appropriate sky background spectrum. For the final sky background spectrum we selected spaxels where no emission lines were detected visually around the wavelength range of interest, but we did not detect line emission for the fibres at the edge of the field. Hence, an over-subtraction of the extended emission should be a small effect.

Both data sets were flux calibrated by comparison with observations of spectrophotometric standard stars observed at the same nights and with the same setup as used for the objects.

3. Results

This section presents the results obtained for each of the RLQs. For reference, the one-dimensional spectra of each QSO created from the data cubes are shown in Fig. 1.

To detect the EELRs it is first necessary to subtract the nuclear QSO emission because this is by far the dominant contribution. To get a clean spectrum of the EELR emission we use the approach described in Sánchez et al. (2004) and (Sánchez et al. 2006). First, a two-dimensional model of the

| Name | alias | redshift | date | instrument | exposure time (s) | seeing (arcsec) |
|--------|------------|----------|------------|------------|-------------------|-----------------|
| OI 363 | Q0738+313 | 0.63 | 2003-04-27 | PMAS | 2×1800 | 0.8 |
| | | | 2003-04-30 | PMAS | 2×1800 | 1.2 |
| | | | 2004-01-16 | INTEGRAL | 4×1800 | 1.0–1.2 |
| 3C 196 | Q0809+4822 | 0.871 | 2004-01-16 | INTEGRAL | 8×1800 | 1.0–1.5 |
| 3C 336 | Q1622+236 | 0.927 | 2003-04-27 | PMAS | 6×1800 | 1.0 |

Table 1. Log of the observations. The observations for 3C 196 were obtained in non-photometric conditions and all derived fluxes are relative.

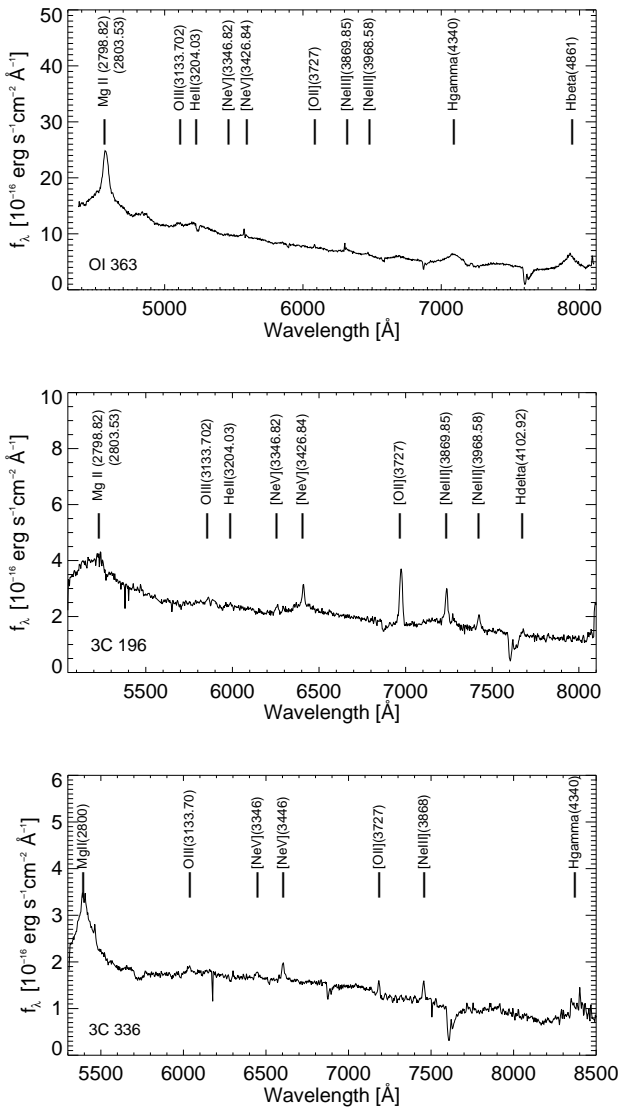


Fig. 1. One-dimensional spectra of the quasars extracted from the data cubes, by co-adding spectra from 20–30 spaxels. Emission lines have been indicated.

QSO PSF is made for each slice in the data cube with a one-pixel width using the program GALFIT (Peng et al. 2002). We allow both a point source representing the continuum (Gaussian component), and an extended host galaxy component to be present, but find that the host component is not detected in any of the objects. Assuming that the spatial loca-

tion of the QSO emission varies smoothly with wavelength we make a model PSF in the form of a data cube. This model data cube is subtracted from the original data to create a residual data cube.

3.1. 3C 196

This is a steep-spectrum, lobe-dominated RLQ (Pooley & Henbest 1974), with a pronounced bend of the radio emission at the location of the hot spots (Brown et al. 1986). Extended oxygen emission has previously been reported based on long-slit spectroscopic observations (Fabian et al. 1988), and the [O II] and [O III] emission ratio was interpreted as a cooling flow (Crawford & Fabian 1989). Optical images in the continuum and a 28 Å wide narrow-band [O II] image showed extensions predominantly to the north-west and south-east (Ridgway & Stockton 1997). The extension to the south-east is mainly caused by an intervening galaxy at $z = 0.4367$ which is responsible for a strong absorption line system in spectrum of the background QSO (Boisse & Boulade 1990).

The INTEGRAL data cube of this object clearly shows extended [O II] emission, even in the frame where the QSO emission is not subtracted. After subtracting the QSO emission, residuals from the QSO are still present due to uncertainties in the wavelength dependent PSF determination, but this effect is strong for only the central region as shown in Fig. 2. The two radio hot-spots found at 5 GHz with a separation of 5.8' at P.A. $\approx 120^\circ$ (Pooley & Henbest 1974) are indicated by the “+” signs. The line emission is predominantly located in two regions as noted before, and the morphology is similar to the [O II] narrow band image presented in Ridgway & Stockton (1997). The north-western part of the nebula appears to have a continuum counterpart which extends to about 2'' from the QSO (Boisse & Boulade 1990; Ridgway & Stockton 1997), but the IFS data is not sensitive to the continuum. North of the quasar we find that the line emission extends out to 3'' (22 kpc), while a brighter region extends 5'' (36 kpc) to the south. Here and throughout we have assumed a flat cosmology with $H_0 = 70 \text{ km s}^{-1} \text{ Mpc}^{-1}$, $\Omega_m = 0.3$ and $\Omega_\Lambda = 0.7$.

Co-adding all the spectra associated with the extended emission after the QSO emission is subtracted results in an emission line with a total flux of $1.2 \times 10^{-15} \text{ erg cm}^{-2} \text{ s}^{-1}$ with a $FWHM$ of $650 \pm 180 \text{ km s}^{-1}$. The width [O II] does not vary significantly over the face of the nebula within the uncertainties of the emission line $FWHM$. However, it is expected that a

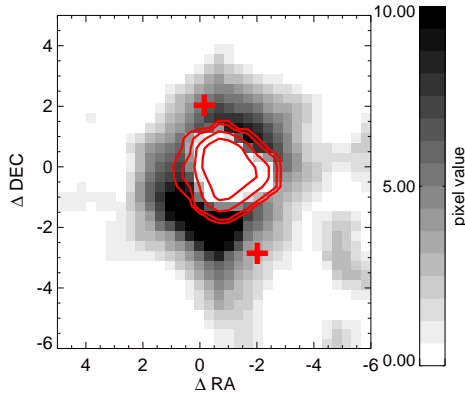


Fig. 2. A narrow-band image of the [O II] emission at $z = 0.871$ (6954–6990 Å) from 3C 196 interpolated to a grid scale of $0''.3$. The axes are given in arcseconds, and the gray scaling is relative. Residuals from the QSO subtraction are present at the central region, which corresponds to three spaxels. Contours of an image at 7000–7050 Å are overlaid, and the QSO centre is located at $(-1, -1)$. The innermost contour corresponds to the FWHM of the QSO PSF. The '+' signs denote the positions of the radio hot spots.

jet-cloud interaction would result in an increased velocity dispersion at the location of the hot spots. With the current data we can not detect this. Higher spatial resolution data are needed to determine if this is the case.

Besides [O II] emission, we also detect extended [Ne III] $\lambda 3869$ emission associated with the brightest [O II] region to the south of the QSO, as shown in the extracted one-dimensional spectrum in Fig. 3. This is similar to the long-slit spectrum presented in Steidel et al. (1997). The extension of the [Ne III] nebula appears smaller than for the [O II] region, but the signal-to-noise level does not allow for a detailed analysis. The emission line ratio $\log([Ne\,III]/[O\,II]) \approx -0.6 \pm 0.1$ is larger than observed for H II regions in the Large Magellanic Cloud (Oey et al. 2000), where values between -1.6 and -0.7 are found, indicating that the ionising flux is harder around the RLQ. Compared to a few other radio-loud objects (Stockton et al. 2002; Solórzano-Iñarrea & Tadhunter 2003), it shows a similar line ratio. We note that the two emission line *FWHM* are very different; 20 ± 1 Å for [O II], while [Ne III] is barely resolved (2.7 ± 3.3 Å when corrected for the instrument resolution). This could signify that the emission originates in different volumes, in which case the line ratio has no physical meaning. Alternatively, a jet-cloud interaction could significantly increase the *FWHM* of the [O II] line at the location of the hot spots, while the [Ne III] only arises from the brighter part of the nebula.

To check for the presence of fainter extended emission farther away than $5''$ from the quasar centre, 30 spectra are co-added at several spatial locations. From the non-detections of emission lines, we derive an upper limit for emission in the surrounding field of $\sim 1 \times 10^{-17}$ erg cm $^{-2}$ s $^{-1}$ arcsec $^{-2}$ in the INTEGRAL data. Not surprisingly, we neither find continuum emission farther than $5''$ from the QSO.

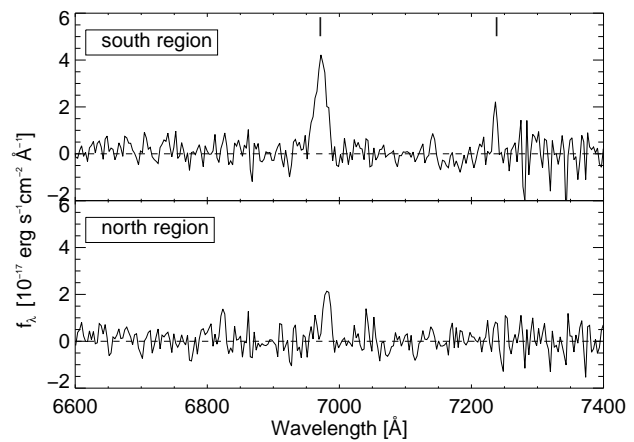


Fig. 3. One-dimensional spectrum of the brightest region to the south of 3C 196 where both [O II] and [Ne III] emission appear extended. These lines are indicated by the vertical lines. The lower panel shows a one-dimensional spectrum of the northern region where no [Ne III] emission is detected.

The spectra from various fibres show that the extended emission around the QSO is progressively shifted in wavelength. Fitting Gaussian profiles to the individual spectra gives evidence for systematic velocity structure over the nebula, as shown in the upper panel of Fig. 4. Only spectra with [O II] detections larger than 2σ above the background are shown in colour. Compared to the systemic redshift of the QSO, the bright southern region has a relative blueshift of -360 km s $^{-1}$, whereas the fainter north western region is redshifted by up to $+500$ km s $^{-1}$. Another representation in the lower panel in Fig. 4 shows a grey scale map of the intensity in the [O II] line emission region derived by fitting emission lines in individual spectra, and the velocity structures of the emission are indicated by contours.

Because our observing campaign was targeted towards finding emission from a $z = 0.4367$ galaxy responsible for the damped Ly α (DLA), the wavelength coverage is not optimal compared to similar studies of other QSOs, which use the [O II]/[O III] ratio to derive an internal gas pressure (e.g. Crawford & Vanderriest 2000). Therefore the present data cube does not allow modeling of the ionising conditions in the nebulae.

The position of the EELR is not exactly aligned with the hot spots to the one arcsec accuracy. However, when we consider that the spectra do not sample the emission contiguously, both the position of the northern and the southern radio hot-spots are spatially coincident with the brightest emission line regions. The southern lobe is associated with the blueshifted emission, and the northern one with the redshifted part. This presents strong indications for an interaction with the radio jets. However, without polarization measurements from each hot spot we do not have the information on which is the nearest, and hence not completely rule out in-flow of the surrounding gas.

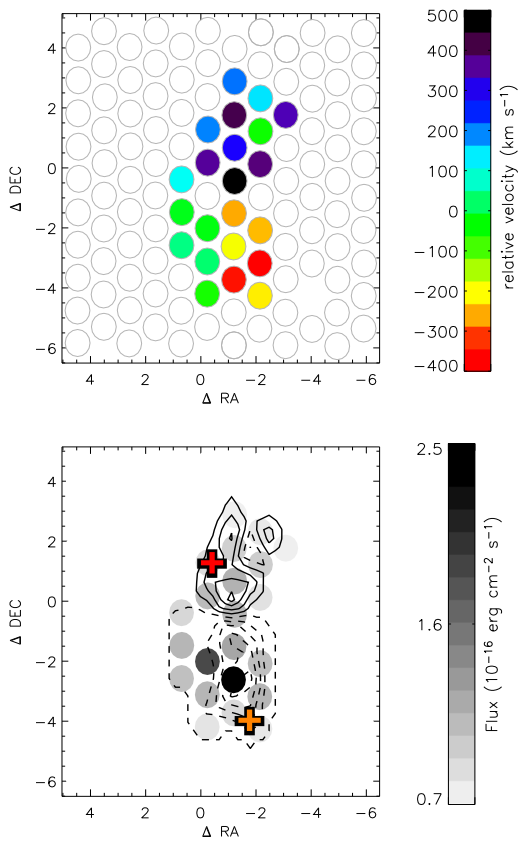


Fig. 4. Upper panel: Velocity structures of the extended [O II] emission around 3C 196 determined after the QSO emission was subtracted. The zero-point of the velocity is the QSO redshift. Outlined circles indicate the spectra where no [O II] emission lines could be fit due to their low signal-to-noise levels. One spaxel close to the QSO centre has not been fitted, because the emission line is affected by QSO subtraction residuals. [See the online edition of the *Journal for a colour version of this figure.*] Lower panel: Image of the [O II] line emission intensity around 3C 196 with velocity contours overlaid. Contour levels are separated by 100 km s^{-1} and negative velocities are shown by the dashed lines. The “+” signs indicate the positions of the two radio hot-spots which are roughly spatially coincident with the brightest emission line regions.

A galaxy responsible for the DLA line at $z = 0.4367$ has been detected $1''.5$ to the south-east of the QSO (Boisse & Boulade 1990; Le Brun et al. 1997; Chen et al. 2005). At this redshift the H β emission line falls close to the [O II] line at the QSO redshift, and so potentially the south-western emission could originate from this DLA galaxy. However, it is unlikely that the brightest region of emission to the south is contaminated; the most likely source for the emission is the QSO environment.

3.2. OI 363

This is a core-dominated, flat spectrum RLQ (Stanghellini et al. 1997). Chandra X-ray observations

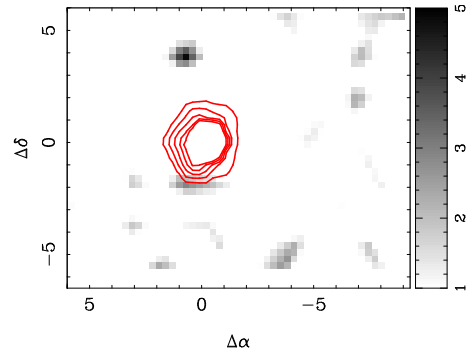


Fig. 5. Narrow-band image of OI 363 created from the INTEGRAL data at $6070 < \lambda < 6090 \text{ \AA}$ which includes [O II] at $z = 0.63$. The scaling has been chosen to show features brighter than 2σ above the background noise, and no EELR features surrounding the quasar are detected. The small features visible in this image are not significant, i.e. they have no associated emission line in an extracted one-dimensional spectrum at this wavelength. The contours show an off-band narrow-band image of the QSO centered at (0,0) where the innermost contour represents the seeing $FWHM$. Because of cross talk between spectra positioned next to each other on the CCD, the QSO PSF appears non circular.

have revealed an X-ray jet with several knots extending to the south-east of the quasar (Siemiginowska et al. 2003). The end of the X-ray jet at 200 kpc is spatially coincident with the weaker extended radio emission.

The [O II] emission line is within the wavelength range of the IFS observations, but a subtraction of the QSO emission from the IFS data cubes reveals no extended emission in either data sets. A narrow-band image created from the INTEGRAL data cube at the wavelength region around [O II] at $z = 0.63$ with a width of 20 \AA is shown in Fig. 5. No bright regions with associated emission lines are found. Other narrow-band images offset by up to 1000 km s^{-1} relative to the quasar redshift show no line emission regions either. We also note that the nuclear [O II] emission line shown in Fig. 1 appears weak. We estimate an upper detection limit for extended [O II] emission of about $3 \times 10^{-17} \text{ erg cm}^{-2} \text{ s}^{-1} \text{ arcsec}^{-2}$ in the INTEGRAL data set and $2 \times 10^{-17} \text{ erg cm}^{-2} \text{ s}^{-1} \text{ arcsec}^{-2}$ in the PMAS data set, based on experiments with artificial emission lines.

Hutchings (1992) obtained broad-band and narrow-band images centered on the [O II] emission line at the quasar redshift and found evidence for a detached region of [O II] emission approximately $2''$ in size and offset by $\sim 3''$ to the north-east. By creating a narrow-band image from the data cube with the same wavelength range as in Hutchings (1992) we search for this detached object, but it is not detected in our data.

3.3. 3C 336

3C 336 is a steep-spectrum lobe-dominated RLQ with radio lobes separated by $28''$ at $\text{PA} \approx 30^\circ$ and a jet extending to the south-east of the QSO (Pooley & Henbest 1974; Bridle et al. 1994). Both Bremer et al. (1992a) and Steidel et al. (1997) reported extended [O II] emission at $z = 0.927$ to the north and

south of the QSO. This emission, detected out to a distance of $5''$ from the core, was previously interpreted as due to a cooling flow (Bremer et al. 1992a), while Steidel et al. (1997) found that it belonged to a blob without a continuum counterpart. The quasar is located in a region where many galaxies are present close to the sight-line. Most of the galaxies are intervening, but seven galaxies have redshifts consistent with being associated with a cluster at $z = 0.923$, i.e. at the quasar redshift (Steidel et al. 1997).

Fig. 6 shows a narrow-band image created from the PMAS data cube. The morphology of the emission region is similar to the 28 \AA wide $[\text{O II}]$ narrow-band image presented in Ridgway & Stockton (1997), but like these authors we cannot confirm the extended emission reaching towards the north. The extended emission region appears to the south and north-west of the QSO, with the brightest region towards the south. The latter is spatially coincident with the radio jet, whereas the north-west emission line region is not aligned.

The PMAS data only allows detection of the emission to $\sim 2''$ from the QSO, and a detailed analysis of the kinematics of the emission line region is not possible with the signal-to-noise level in each individual spectrum from the data cube. In the co-added one-dimensional spectrum for the whole emission line region the total line flux measured is $(3.8 \pm 1.4) \times 10^{-16} \text{ erg cm}^{-2} \text{ s}^{-1}$ after a correction for Galactic extinction is applied (Schlegel et al. 1998). After correcting for the instrumental resolution, the line width is $910 \pm 280 \text{ km s}^{-1}$.

A narrow-band image from the data cube, offset to slightly longer wavelengths ($7190\text{--}7206 \text{ \AA}$) shows that the emission feature extends further to the north-west and is spatially coincident with the emission feature denoted ‘2’ in a continuum image of Steidel et al. (1997), which is marked by ‘+’ in Fig. 6. A one-dimensional spectrum of that region in the data cube indicates $z = 0.9300 \pm 0.0009$, in agreement with $z = 0.931$ measured by Steidel et al. (1997). Furthermore, the data cube allows a confirmation of their object ‘3’ at $z = 0.892$, $3''$ to the east of the QSO. Possibly, the emission to the north-west is unrelated to the QSO and only belongs to the galaxy ‘2’; thus we determine the properties of the southern region only. Here the flux is $1.8 \pm 0.5 \times 10^{-16} \text{ erg cm}^{-2} \text{ s}^{-1}$ and the $FWHM$ is $720 \pm 200 \text{ km s}^{-1}$. The redshift measured is $z = 0.9274 \pm 0.0007$, corresponding to a velocity difference of $60 \pm 110 \text{ km s}^{-1}$ relative to the QSO redshift.

4. Discussion and conclusions

We have presented integral field spectroscopy of three RLQs, where one is core-dominated and the other two are lobe-dominated. Extended $[\text{O II}]$ emission is seen around the two lobe-dominated RLQs, and the emission is spatially coincident with the radio emission. All lines from the EELRs are relatively narrow with $FWHM < 1000 \text{ km s}^{-1}$. The brightest object (3C 196) has an EELR velocity structure which changes by more than 800 km s^{-1} over approximately 60 kpc.

Compared to the other RLQs where an alignment has been detected (Crawford & Vanderriest 2000, e.g.), the EELR around 3C 196 suggests the presence of a jet-cloud interaction with strong velocity differences. The emission line neb-

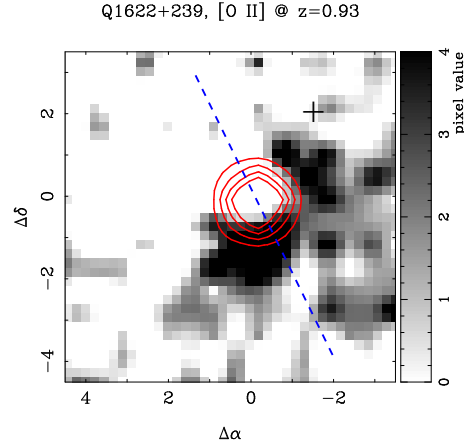


Fig. 6. Narrow-band image of the $[\text{O II}]$ line emission region from 3C 336 in the region $7167\text{--}7193 \text{ \AA}$. The image is interpolated to a pixel scale of $0''.2$ to make visible the faint emission. The field of view is $8''\text{--}8''$, north is up and east to the left. The location of the object denoted ‘2’ in Steidel et al. (1997) is marked by the ‘+’ sign. A narrow-band image at slightly redder wavelengths ($7190\text{--}7206 \text{ \AA}$) shows emission at larger distances than in this image, which is consistent with the $2''.58$ offset reported in Steidel et al. (1997). Contours show an off-band narrow-band image ($6950\text{--}7000 \text{ \AA}$) where the innermost contour represent the seeing $FWHM$. The dashed line represents the orientation of the radio jet which extends beyond the field of view of the IFS data.

ula has both a red- and a blueshifted component aligned with the radio hot spots, and the velocity is larger than expected for a gravitational origin. Rotation velocities for the most rapidly rotating massive spiral disks are around 300 km s^{-1} at a distance of about 10 kpc. If the EELR is a rotating disk, its mass would have to be at least twice that of such a massive spiral. The bend of the radio emission at the location of the hot spots noted in Brown et al. (1986) supports the interpretation of an interaction. The $[\text{O II}]$ emission from the galaxy is spatially offset from the intervening galaxy found by Boisse & Boulade (1990), which at a redshift of 0.87 has $\text{H}\beta$ emission lines very close to the $[\text{O II}]$ at the QSO redshift. With emission line fitting we are able to separate the $\text{H}\beta$ emission line from the $[\text{O II}]$ emission, because there is a 10 \AA difference between the two lines, and the positions are not exactly spatially coincident.

Extended $[\text{Ne III}]$ emission is detected for 3C 196 at a distance of 30 kpc from the quasar nucleus, but only in the southern region where the $[\text{O II}]$ emission is strongest. Because the $[\text{Ne III}]/[\text{O II}]$ line flux ratio is larger than observed in H II regions, harder ionising radiation must be present if the emission originates in the same volume. For a detailed modeling more emission lines need to be observed. Ionisation conditions can in principle be analysed in the EELRs provided that the $[\text{O III}]$ emission line is detected too. Combining the observed emission line ratios with knowledge of the quasar ionising flux allows determination of the nebular pressure through photoionisation modeling. However, this approach is only justified when emission lines arise in the same medium. This is sometimes neglected, as pointed out by Stockton et al. (2002), who find that

the [O II] emission arises in a much denser medium than [O III] in one RLQ. Measurements of other line ratios could help to determine the nature of the nebulae and the presence of interaction signatures (e.g. Garcia-Lorenzo et al. 2005).

The alignment of the nebular emission line regions with the radio jets indicates that some interaction could be present. To determine whether the line emission is created by the ionising quasar flux which is collimated along the radio jet, it is necessary to determine the underlying continuum flux. If a significant stellar emission component is present then one can rule out this scenario. No extended continuum emission is detected in either object analysed here, but if it were present, the bright nuclear flux complicates the detection. Deeper (imaging) data could resolve this issue. Furthermore, if the extended emission is caused by an interaction with the radio jet, larger field of view observations of 3C 336 are necessary to analyse the effects at larger distances corresponding to the widely separated radio-lobes.

In the unification scheme, the core-dominated RLQs have their radio jet orientation closely aligned with the sight line. If radio jets cause interaction with the surrounding material and give rise to line emission, a core-dominated RLQ would have less extended emission than lobe-dominated RLQs. No EELR is detected for the one core-dominated RLQ analysed here.

An alternative scenario where the extended emission is dominated by the QSO ionising radiation directed in a cone (Haiman & Rees 2001; Weidinger et al. 2005) can not be rejected completely on the basis of this investigation. However, the velocity structure of the nebulae around 3C 196 supports the hypothesis that it is the interaction of the material with the radio jet which is the dominant effect and causes an outflow of the material.

Acknowledgements. L. Christensen acknowledges support by the German Verbundforschung associated with the ULTROS project, grant no. 05AE2BAA/4. S.F. Sánchez and K. Exter acknowledge the support from the Euro3D Research Training Network, grant no. HPRN-CT2002-00305. K. Jahnke acknowledges support from DLR, project no. 50 OR 0404.

References

Arribas, S., Carter, D., Cavaller, L., et al. 1998, in Proc. SPIE Vol. 3355, Optical Astronomical Instrumentation, Sandro D'Odorico; Ed., 821–827

Barthel, P. D. 1989, *ApJ*, 336, 606

Becker, T. 2002, PhD thesis, Astrophysikalisches Institut Potsdam, Germany

Boisse, P. & Boulade, O. 1990, *A&A*, 236, 291

Bremer, M. N. 1997, *MNRAS*, 284, 126

Bremer, M. N., Crawford, C. S., Fabian, A. C., & Johnstone, R. M. 1992a, *MNRAS*, 254, 614

Bremer, M. N., Fabian, A. C., Sargent, W. L. W., et al. 1992b, *MNRAS*, 258, 23

Bridle, A. H., Hough, D. H., Lonsdale, C. J., Burns, J. O., & Laing, R. A. 1994, *AJ*, 108, 766

Brown, R. L., Broderick, J. J., & Mitchell, K. J. 1986, *ApJ*, 306, 107

Chen, H.-W., Kennicutt, R. C., & Rauch, M. 2005, *ApJ*, 620, 703

Christensen, L., Sanchez, S. F., Jahnke, K., et al. 2004, *A&A*, 417, 487

Christensen, L., Schulte-Ladbeck, R. E., Sánchez, S. F., et al. 2005, *A&A*, 429, 477

Crawford, C. S. & Fabian, A. C. 1989, *MNRAS*, 239, 219

Crawford, C. S. & Vanderriest, C. 1997, *MNRAS*, 285, 580 —. 2000, *MNRAS*, 315, 433

Di Matteo, T., Springel, V., & Hernquist, L. 2005, *Nature*, 433, 604

Fabian, A. C. & Crawford, C. S. 1990, *MNRAS*, 247, 439

Fabian, A. C., Crawford, C. S., Johnstone, R. M., Hewett, P. C., & Allington-Smith, J. R. 1988, *MNRAS*, 235, 13P

Garcia-Lorenzo, B., Sánchez, S. F., Mediavilla, E., González-Serano, J. I., & Christensen, L. 2005, *ApJ*, 621, 146

Haiman, Z. & Rees, M. J. 2001, *ApJ*, 556, 87

Heckman, T. M., Miley, G. K., Lehnert, M. D., & van Breugel, W. 1991, *ApJ*, 370, 78

Hutchings, J. B. 1992, *AJ*, 104, 1311

Le Brun, V., Bergeron, J., Boisse, P., & Deharveng, J. M. 1997, *A&A*, 321, 733

Márquez, I., Pécontal, E., Durret, F., & Petitjean, P. 2000, *A&A*, 361, 5

McCarthy, P. J., van Breugel, W., Spinrad, H., & Djorgovski, S. 1987, *ApJ*, 321, L29

Oey, M. S., Dopita, M. A., Shields, J. C., & Smith, R. C. 2000, *ApJS*, 128, 511

Peng, C. Y., Ho, L. C., Impey, C. D., & Rix, H.-W. 2002, *AJ*, 124, 266

Pooley, G. G. & Henbest, S. N. 1974, *MNRAS*, 169, 477

Pych, W. 2004, *PASP*, 116, 148

Ridgway, S. E. & Stockton, A. 1997, *AJ*, 114, 511

Roth, M. M., Bauer, S., Dionies, F., et al. 2000, in Proc. SPIE, Vol. 4008, 277–288

Roth, M. M., Kelz, A., Fechner, T., et al. 2005, *PASP*, 117, 620

Sánchez, S. F. 2004, *AN*, 325, 167

Sánchez, S. F., García-Lorenzo, B., Jahnke, K., et al. 2006, *New Astronomy Review*, 49, 501

Sánchez, S. F., García-Lorenzo, B., Mediavilla, E., González-Serrano, J. I., & Christensen, L. 2004, *ApJ*, 615, 156

Schlegel, D. J., Finkbeiner, D. P., & Davis, M. 1998, *ApJ*, 500, 525

Siemiginowska, A., Stanghellini, C., Brunetti, G., et al. 2003, *ApJ*, 595, 643

Solórzano-Iñarrea, C. & Tadhunter, C. N. 2003, *MNRAS*, 340, 705

Stanghellini, C., O'Dea, C. P., Baum, S. A., et al. 1997, *A&A*, 325, 943

Steidel, C. C., Dickinson, M., Meyer, D. M., Adelberger, K. L., & Sembach, K. R. 1997, *ApJ*, 480, 568

Stockton, A. & MacKenty, J. W. 1987, *ApJ*, 316, 584

Stockton, A., MacKenty, J. W., Hu, E. M., & Kim, T. 2002, *ApJ*, 572, 735

Turnshek, D. A. 1984, *ApJ*, 280, 51

Villar-Martin, M., Tadhunter, C., & Clark, N. 1997, *A&A*, 323, 21

Weidinger, M., Møller, P., Fynbo, J. U., & Thomsen, B. 2005,

A&A, 436, 825

Wilman, R. J., Johnstone, R. M., & Crawford, C. S. 2000,

MNRAS, 317, 9